



Entropy-based bilateral filtering with a new range kernel

Tao Dai, Weizhi Lu*, Wei Wang, Jilei Wang, Shu-Tao Xia

Graduate School at Shenzhen, Tsinghua University, Shenzhen, Guangdong province, 518055, China



ARTICLE INFO

Article history:

Received 11 August 2016

Revised 7 January 2017

Accepted 11 February 2017

Available online 13 February 2017

Keywords:

Image denoising

Bilateral filter

Method noise

Local entropy

ABSTRACT

Bilateral filter (BF) is a well-known edge-preserving image smoothing technique, which has been widely used in image denoising. The major drawback of BF is that its range kernel is sensitive to noise. To address this issue, we propose an entropy-based BF (EBF) with a new range kernel which contains a new range distance. The new range distance is robust to noise by exploiting the information from the denoised estimate and the corresponding method noise, i.e., the difference between the noisy image and its denoised estimate. Moreover, in order to consider the local statistics of images, local entropy is applied to adaptively guide the range parameter selections. This allows our method to adapt to the images with different characteristics. Experimental results demonstrate that the proposed EBF significantly outperforms the standard BF in terms of both quantitative metrics and subjective visual quality.

© 2017 Elsevier B.V. All rights reserved.

1. Introduction

Bilateral filter (BF) [1] is a well-known edge-preserving tool, which has been widely used in image denoising. To remove noise while preserving edges, BF uses the weighted average of nearby pixels in a local neighborhood, where weights rely on the spatial and intensity distance. The output of BF centered at \mathbf{q} can be expressed as

$$\hat{y}(\mathbf{q}) = \frac{\sum_{\mathbf{p} \in S} w_{\sigma_s} \cdot w_{\sigma_r} \cdot y(\mathbf{p})}{\sum_{\mathbf{p} \in S} w_{\sigma_s} \cdot w_{\sigma_r}}, \quad (1)$$

where $y(\mathbf{p})$ is the noisy pixel, and S is the neighborhood of size $(2r+1) \times (2r+1)$ centered at \mathbf{q} ; w_{σ_s} and w_{σ_r} are the spatial kernel and range kernel, both of which determine the practical performance of BF. More precisely,

$$w_{\sigma_s} = \exp \left(-\frac{\|\mathbf{p} - \mathbf{q}\|_2^2}{2\sigma_s^2} \right), \quad (2)$$

where the spatial distance $\|\mathbf{p} - \mathbf{q}\|_2^2$ measures the spatial correlations and the spatial parameter σ_s controls the size of the spatial neighborhood, and

$$w_{\sigma_r} = \exp \left(-\frac{|y(\mathbf{p}) - y(\mathbf{q})|^2}{2\sigma_r^2} \right), \quad (3)$$

where the range distance $|y(\mathbf{p}) - y(\mathbf{q})|^2$ measures the intensity correlations and the range parameter σ_r controls how much a nearby pixel is weighted due to the pixel intensity.

The denoising performance of BF is mainly determined by the range kernel rather than the spatial kernel, which was demonstrated in [2]; hence we focus hereafter on the improvement of the range kernel. As stated above, the range kernel contains two crucial factors, i.e., the range distance and range parameter. However, both of these factors are sensitive to noise. Thus many research efforts have concentrated on how to obtain a good estimation of these two factors under various noise levels.

The conventional range distance is computed directly from noisy images. This, however, leads to large estimation bias due to the seriously corrupted correlations of pixels under strong noise. Some invariants [3–6] of BF attempted to alleviate the estimation bias by calculating the range distance from denoised images. However, these methods still cannot achieve satisfying results under strong noise, since the denoised images are usually far away from the original ones. Moreover, from the analysis of method noise¹ [7], the denoised image does not contain the complete details. In other words, there still exist the *residual image structures* (the original image structures) in method noise. As a result, the estimation accuracy of the range distance can be further improved, if we can exploit the local similarities of the residual image structures.

Besides, many research works focus on tuning the range parameter. Some recently developed adaptive bilateral filters (ABFs) [2,8,9] have adapted the range parameter to the global [2,8] or local structures of the images [9]. Among them, Zhang et al. [2] demonstrated that the range parameter has more impact on the denoising performance than the spatial parameter, and showed that

* Corresponding author.

E-mail addresses: dait14@mails.tsinghua.edu.cn (T. Dai), wzlsd@sz.tsinghua.edu.cn (W. Lu).

¹ Method noise is often defined as the difference between the noisy image and its corresponding denoised image.

the optimal range parameter is linearly proportional to the standard deviation of the noise, i.e., $\sigma_r = k \cdot \sigma$, where k is a fixed value chosen empirically. Using such globally fixed range parameter may lead to unsatisfying results for the images with various structures, such as *Barbara*, since the global range parameter cannot consider the local structures. More recently, a new ABF [9] with spatially adaptive parameter selections has been proposed, which, however, requires high computational complexity. Therefore, it is still demanding to propose a novel BF with spatially adaptive parameter selections and low complexity.

Motivated by the above observations, we propose an adaptive entropy-based BF (EBF) with a new range kernel which includes a new range distance. To be specific, the new range distance is estimated from a “clean” image, which is derived by exploiting the information both from the denoised estimate and the residual image in method noise. Compared with the range distance estimated from the noisy or denoised image, ours is more robust to various noise levels. Furthermore, in order to consider the structural characteristics of the images, local entropy serves as a guide for adaptive range parameter selections. In information theory, local entropy represents the variance of local regions and catches the natural properties of transition regions of edges. Based on this fact, our method builds a set of entropy-based local image descriptors, extracted from the noisy image and used to modulate the range parameter across the image. Unlike the above-mentioned methods [2,8,9] which learn the optimal filter parameters with high complexity, our method obtains adaptive range parameters at a local scale with a relatively low complexity. To apply the proposed EBF for image denoising, a two-stage EBF based framework is presented, which is detailed in Fig. 4. In summary, the main contributions of the paper are as follows:

1. A new range distance is estimated from a “clean” image, which exploits the information from the denoised image and the residual image in method noise.
2. A simple but effective approach is proposed to adaptively tune the range parameter, which applies local entropy to characterize the local structures of images.

The rest of this paper is organized as follows. Section 2 briefly reviews the related works, including the major image denoising methods and the existing progress of bilateral filter. In Section 3, we introduce the basic concepts of method noise and local entropy. In Section 4, we propose an EBF-based denoising framework. Section 5 shows the experimental results. Finally, we draw the conclusions.

2. Related works

In general, image denoising methods can be divided into three categories: spatial domain, transform domain and learning-based denoising methods [10], where BF belongs to spatial domain methods. In this section, we briefly review the major methods for image denoising and the main previous works related to BF.

Spatial domain methods attempt to utilize the correlations of natural images [11]. According to the selection of pixels (patches), spatial filters can be categorized as local and nonlocal filters. Local filters are restricted in a local spatial distance, such as Gaussian filtering, anisotropic filtering [12], total variation minimization (TV) [13,14] and joint filtering [15]. However, these methods cannot perform well at high noise levels because the correlations between neighboring pixels are corrupted by the severe noise. To overcome this issue, the nonlocal filters utilize the self-similarity of natural images in a nonlocal manner. Nonlocal means (NLM) filter [7], achieves a denoised pixel by weighted averaging all other pixels in the noisy image, whose pixel similarity depends on the patch. The main drawback of NLM filters is that these

patch-based methods are computational-intensive and often tend to over-smooth image details. More recently, the idea of nonlocal similarity has been extended to transform domain [16–18] and learning-based methods [19–21] in order to further improve the denoising performance. Among them, learning-based method proposed by Elad et al. [19] obtained good results based on sparse and redundant representations over learned dictionaries. Besides, the so-called BM3D [16] achieved remarkable results by combining the patch-based techniques like NLM with transform-based filtering. Beyond utilizing the nonlocal prior, some important works can also obtain remarkable results by utilizing low-rank prior of images, such as WNNM [22]. In a different direction, it was observed in [23,24] that neural networks can be successfully applied to image denoising.

Besides the above patch-based methods, BF has received much attention due to its simplicity and efficiency. Most BF-based methods can be roughly divided into two lines of work, i.e. theoretical analysis and performance improvement.

Some theoretical works of BF deserve mentioning. In [25], it was demonstrated that BF emerges from Bayesian approach and is identical to the first iteration of Jacobi algorithm. Barash et al. [26] related BF with anisotropic diffusion (AD) [12]. Besides, the relationship between BF and TV regularization was developed in [27], which was further generalized by casting BF, median filters, mode filtering, nonlinear diffusion filtering, and regularization techniques in a single unified framework of discrete regularization theory in [28]. In a different direction, Takeda et al. [29] observed that BF is a simple example of kernel regression. Recently, Caraffa et al. [30] proposed an iterated version of BF that is robust to outliers and demonstrated how it can be used to remove non-Gaussian noise.

More works focus on the performance improvement of BF, including parameter selection and acceleration. For parameter selection, Zhang and Gunturk [2] demonstrated that the optimal σ_s is relatively insensitive to the noise standard deviation σ and it is generally in the range [1.5, 2.1], while the range parameter σ_r has more impact on the denoising performance. Based on the experimental results obtained on a large set of natural images, Zhang and Gunturk suggested that the optimal σ_r should be approximately linearly related to σ . Another ABF [8] for sharpness enhancement and noise removal used a complex training procedure to optimize the filter parameters. In addition, many works have been done to accelerate BF. A direct computation of BF requires $O(r^2)$ operations per pixel. To speed up BF, researchers have come up with several fast algorithms [31–37]. Durand et al. [31] sped up BF based on a piecewise-linear approximation in the intensity domain and subsampling in the spatial domain. In addition, it was observed in [32] that BF can be considered as a linear filter acting in three-dimensions, where the three-dimensions are obtained by augmenting the image intensity to the spatial dimensions. The algorithm in [33] enabled bilateral filtering in constant time $O(1)$ without sampling, which was further improved by using trigonometric range kernels in [34,35]. More recent works like [36,37] further accelerated BF by approximating the range kernel using polynomial and trigonometric functions.

3. Fundamentals

3.1. Method noise

Given a gray-level image \mathbf{y} contaminated with additive white Gaussian noise (AWGN), i.e.,

$$\mathbf{y} = \mathbf{x} + \mathbf{n}, \quad (4)$$

where \mathbf{x} is the clean image, and \mathbf{n} is AWGN with zero mean and standard deviation σ .

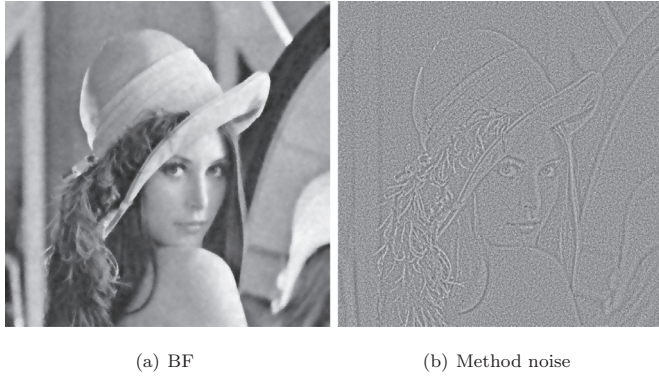


Fig. 1. Denoised result of BF in (a) and its method noise in (b) for the image *Lena* at $\sigma = 20$.

Method noise $\hat{\mathbf{n}}$ is often defined to be the difference between the noisy image and its denoised image, then $\hat{\mathbf{n}}$ can be expressed as

$$\hat{\mathbf{n}} = \mathbf{y} - \hat{\mathbf{y}}, \quad (5)$$

where $\hat{\mathbf{y}}$ is the denoised image of \mathbf{y} .

Method noise is often used to evaluate whether a denoising method has removed too many structures from the input image, and the fewer details we can see in the method noise, the more details have been preserved in the denoised image.

For better understanding, we give an example to show the denoised image of BF and its corresponding method noise in Fig. 1. It can be seen that there still exist rich original image structures in the method noise, which indicates the substantial potential improvement that can be made for the denoising method.

3.2. Local entropy

Given an image with L gray levels, following Shannon's definition of entropy [38], Kapur et al. [39] define the entropy of an image as

$$E(P_0, P_1, \dots, P_{L-1}) = - \sum_{i=0}^{L-1} P_i \log P_i, \quad (6)$$

where $P_i = \frac{N_i}{N}$ is the probability of gray level i appearing in the image, N is the total number of pixels in the image, and N_i is the number of pixels with grayscale i .

Given a pixel in position \mathbf{q} , suppose Ω is a small neighborhood of size $m \times n$ centered at \mathbf{q} , then the local entropy $e(\mathbf{q})$ of Ω is defined to be

$$e(\mathbf{q}) = - \sum_{k=0}^{L-1} p_k \log p_k, \quad (7)$$

where $p_k = \frac{n_k}{m \times n}$ is the probability of gray level k appearing in the neighborhood Ω , and n_k is the number of pixels with gray level k in the neighborhood Ω . Hence, we use a sliding window of size $m \times n$ (e.g. 9×9) to compute the local entropy.

In information theory [38], the entropy function $E(P_0, P_1, \dots, P_{L-1})$ has two important properties:

1. Entropy function $E(P_0, P_1, \dots, P_{L-1})$ takes its largest value for the uniform distribution, i.e.,

$$E(P_0, P_1, \dots, P_{L-1}) \leq E\left(\frac{1}{L}, \frac{1}{L}, \dots, \frac{1}{L}\right).$$

2. We define $\phi(L) = E\left(\frac{1}{L}, \frac{1}{L}, \dots, \frac{1}{L}\right)$, then $\phi(L)$ of a variable L is non-decreasing, i.e.,

$$\phi(L) \leq \phi(L+1).$$

Thus, it can be indicated that the local entropy is relatively small in homogeneous neighborhoods (e.g. background) but relatively large in heterogeneous regions (e.g. area of edges). This fact will give us a useful guide for tuning the parameter of our method.

4. The proposed EBF based denoising framework

As stated before, bilateral filtering is sensitive to the range distance and range parameter. To overcome such limitations, we attempt to utilize the residual image in method noise to improve the robustness of the range distance, and exploit the characteristics of images to adjust the range parameter. As a result, we propose a new range kernel, consisting of a new range distance based on method noise and adaptive range parameter selection based on local entropy.

4.1. A new range distance based on method noise

The conventional BF directly uses the noisy image to estimate pixel similarities. Due to the impact of noise, the range distance usually cannot be reasonably estimated. To address this problem, we try to derive the range distance from the clean image instead of the noisy image. In this section, we show how to compute the pixel similarity between the clean pixels, i.e., the squared Euclidean distance $|x(\mathbf{p}) - x(\mathbf{q})|^2$.

To the end, the clean image can be approximated by the denoised estimate and the residual image. Since we have $\hat{n}(\mathbf{p}) = y(\mathbf{p}) - \hat{y}(\mathbf{p})$, then the pixel of the clean image can be written as

$$\begin{aligned} x(\mathbf{p}) &= y(\mathbf{p}) - n(\mathbf{p}) = (\hat{y}(\mathbf{p}) + \hat{n}(\mathbf{p})) - n(\mathbf{p}) \\ &= \hat{y}(\mathbf{p}) + (\hat{n}(\mathbf{p}) - n(\mathbf{p})) \\ &= \hat{y}(\mathbf{p}) + \Delta x(\mathbf{p}), \end{aligned} \quad (8)$$

where $\Delta x(\mathbf{p}) = \hat{n}(\mathbf{p}) - n(\mathbf{p})$ denotes the residual image in method noise. For simplicity, we assume that method noise \hat{n} contains all the additive noise n due to the smoothing effect of the bilateral filtering, such that the denoised estimate \hat{y} contains no noise². Note that from the previous work in [40], we cannot get good denoising results by simply adding $\Delta x(\mathbf{p})$ back to $\hat{y}(\mathbf{p})$ due to the fact that $\Delta x(\mathbf{p})$ can only be obtained as a coarse approximation.

Based on (8), the pixel similarity between clean pixels $x(\mathbf{p})$ and $x(\mathbf{q})$ is derived as follows

$$\begin{aligned} |x(\mathbf{p}) - x(\mathbf{q})|^2 &= |(\hat{y}(\mathbf{p}) + \Delta x(\mathbf{p})) - (\hat{y}(\mathbf{q}) + \Delta x(\mathbf{q}))|^2 \\ &= |\hat{y}(\mathbf{p}) - \hat{y}(\mathbf{q})|^2 + |\Delta x(\mathbf{p}) - \Delta x(\mathbf{q})|^2 \\ &\quad + 2(\hat{y}(\mathbf{p}) - \hat{y}(\mathbf{q}))(\Delta x(\mathbf{p}) - \Delta x(\mathbf{q})), \end{aligned} \quad (9)$$

where we can see that the contribution of the denoised pixels, i.e., $|\hat{y}(\mathbf{p}) - \hat{y}(\mathbf{q})|^2$ on the right side plays an important role. However, if the other two terms are not zero, the term $|x(\mathbf{p}) - x(\mathbf{q})|^2$ cannot neglect the influence of the second term $|\Delta x(\mathbf{p}) - \Delta x(\mathbf{q})|^2$ and the last term $2(\hat{y}(\mathbf{p}) - \hat{y}(\mathbf{q}))(\Delta x(\mathbf{p}) - \Delta x(\mathbf{q}))$, which exploits the relationship between the residual image and the denoised estimate.

Now let us see how to obtain the residual signal $\Delta x(\mathbf{p})$. Due to the low signal noise ratio (SNR) of method noise, it is difficult to get the residual image $\Delta x(\mathbf{p})$ from the method noise. To reduce the effect of noise, the authors in [40] used an adaptive Wiener filter to denoise the method noise. It is beneficial to use Wiener filter, since it can smooth the noise while preserving the residual image without adding much computational cost. Therefore, we adopt an adaptive Wiener filter to extract the residual image.

² In practice, the denoised estimate \hat{y} still contains some amount of noise due to the imperfect denoising.

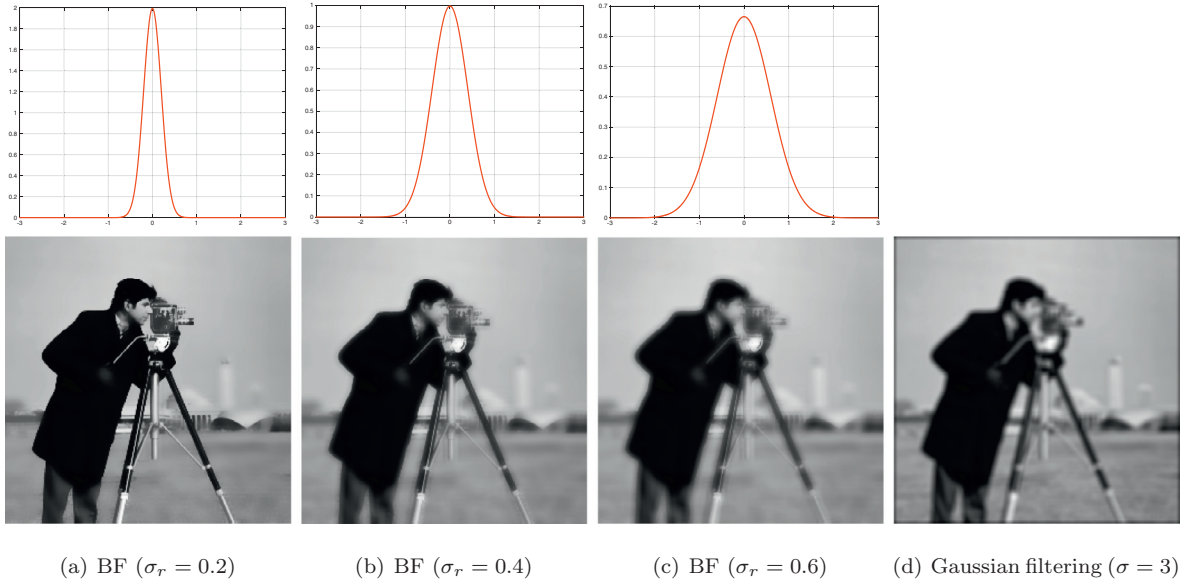


Fig. 2. Examples of BF with different σ_r ($\sigma_s = 5$). Top row shows the profile of a 1D range kernel and bottom row shows the results obtained by the corresponding BF. As σ_r increases, BF gradually approximates Gaussian filtering more closely. The original image intensity values span [0, 1].

Then the new range kernel \hat{w}_{σ_r} is obtained by replacing $|y(\mathbf{p}) - y(\mathbf{q})|^2$ in (3) with $|x(\mathbf{p}) - x(\mathbf{q})|^2$ in (9)

$$\hat{w}_{\sigma_r} = \exp\left(-\frac{|x(\mathbf{p}) - x(\mathbf{q})|^2}{2\hat{\sigma}_r^2}\right), \quad (10)$$

where the range parameter $\hat{\sigma}_r$ controls the amount of filtering, which is estimated in the following parts.

4.2. Adaptive range parameter based on local entropy

The range parameter plays a key role in determining the contrast of features to preserve. As the range parameter increases, BF gradually approximates Gaussian convolution more closely [41]. This is because as the range parameter increases, the range kernel become wider and flatter (see Fig. 2), i.e., is nearly constant over the intensity of the image.

In order to better illustrate the effects of the range parameter, we show plots of the range kernel with different range parameters in Fig. 2. It can be seen that as the range parameter increases, the range kernel widens and flattens. As a result, images are more blurred as σ_r increases. (see Fig. 2(a-c)).

Most of the existing literature uses globally fixed range parameter without considering local structures [2,8] or uses spatially adaptive range parameter with high computational cost [9]. Instead, we propose adaptive range parameter selections in terms of entropy-based local image descriptor with low time complexity.

4.2.1. Entropy-based local image descriptor

Local image descriptors are necessary to appropriately guide the modulation of the filtering parameters across the image. Entropy-based image descriptors have already been used for edge detection [42], and adaptive filters based on local image content [43]. We use entropy-based image descriptor to guide the modulation of the range parameter. From Section 3, we know that local entropy can be applied to represent the local characteristics of an image.

To better illustrate the characteristics of local entropy, for noise-free images in Fig. 3(a-d), Table 1 shows entropies calculated for each image at various noise levels. Specifically, $E = 0$ for the flat area, and $E = 1.0$ for textured area, where grey levels are assumed to be few (only two in this example) different values because of

the regularity of the texture. Whereas $E = 7.0$ in the gradient area and $E = 6.66$ in the complex area, where the grey levels are much more than those in flat and textured areas. This implies that these areas can be distinguished by entropy under the noise-free cases. As noise (e.g. $\sigma = 10$) is added to the images, entropies of these areas will increase to varying degrees. From Table 1, we can see that the entropies of flat and textured areas increase faster than those of gradient and complex areas. This is mainly because entropy function is a non-decreasing function of the grey levels for the uniform distribution. When adding noise, grey levels of flat and textured areas increase much faster than those of gradient and complex areas. As the noise becomes strong (e.g. $\sigma = 40, 50$), the difference of the entropies between these areas becomes smaller. Fig. 3 (e and f) show the local entropy maps for the image Lena, in absence and presence of noise. For an image, the local entropy is computed with a sliding window of size 9×9 at every pixel location. It can be seen that entropies of the heterogeneous areas (e.g. edges) are generally larger than those of the homogeneous areas (e.g. background area) in the absence and presence of noise.

All these above-mentioned results indicate that local entropy can be used to separate the areas of flat, gradient, textured, and complex regions, regardless of the presence of noise or not. Motivated by this fact, we propose an entropy-based way to adaptively tune the range parameter, which is shown in the next section.

4.2.2. Entropy-based range parameter selections

This section focuses on how to determine the range parameter according to the characteristics of the images. As the range parameter increases, BF is more close to Gaussian convolution [41]. Recent works like [2,8] with global range parameter cannot adapt to the images with various structures, such as Barbara, for the global range parameter cannot consider the local structures.

Instead, we seek spatially adaptive range parameter selections by considering the local characteristics of images. As stated before, different areas in images, such as flat, gradient, texture and complex areas, can be distinguished by local entropy. More specifically, images have relatively large local entropy in heterogeneous regions, but relatively small ones in homogeneous areas. Motivated by this fact, we propose a local entropy-based approach to adaptively tuning the range parameter. Specifically, the heteroge-

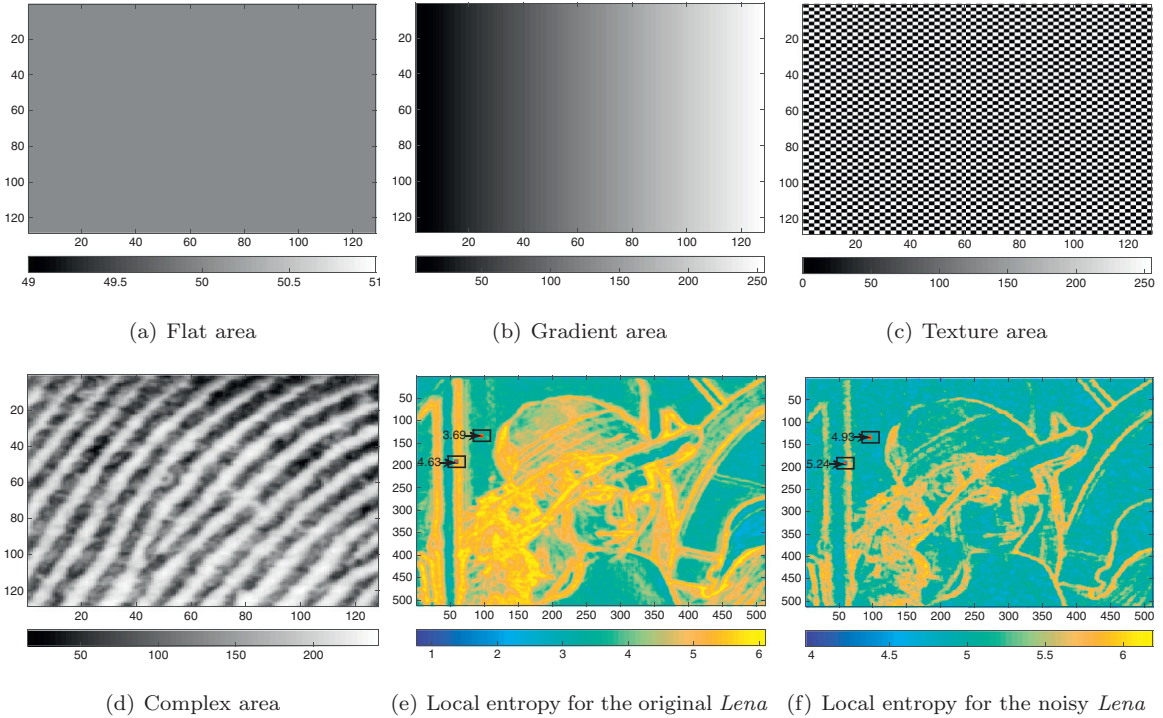


Fig. 3. Panels (a-d) show a 128 × 128 flat, gradient, textured, and complex, noise-free area. Entropies for these images are shown in Table 1. Panels (e-f) show local entropy maps of noise-free and noisy image *Lena*, respectively.

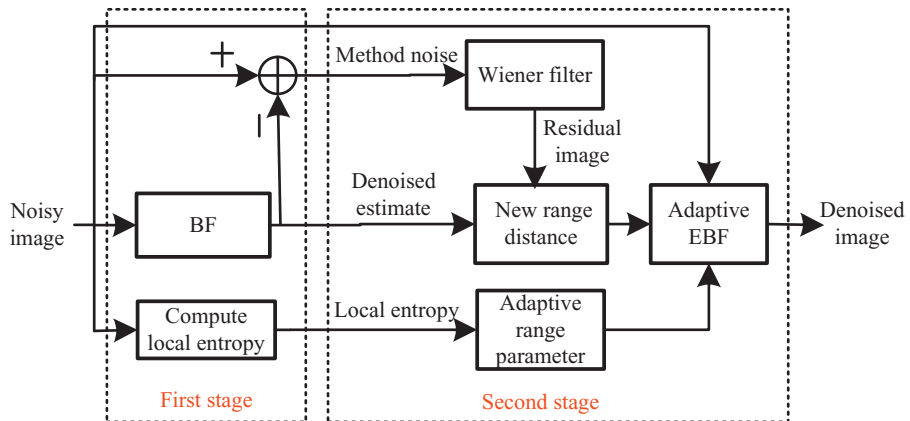


Fig. 4. Diagram of the proposed denoising framework.

Table 1
Entropies (E) for the flat, gradient, texture, and complex images shown in Fig. 3.

σ	0	10							
E	Flat	Gradient	Texture	Complex	Flat	Gradient	Texture	Complex	
0	7.0	1.0	6.66	6.66	3.09	7.95	4.10	7.65	
40	Flat	Gradient	Texture	Complex	50	Flat	Gradient	Texture	Complex
E	6.72	7.60	5.12	7.42	6.69	7.47	5.31	7.69	

neous areas would be fit for relatively smaller range parameter to preserve edges better, while the homogeneous regions would adapt to relatively larger range parameter to remove the noise better.

To this end, we adopt a simple *Sigmoid* function. Then spatially adaptive range parameter $\hat{\sigma}_r$ can be expressed as

$$\hat{\sigma}_r = K(e(\mathbf{q}), \alpha, k, T) \cdot \sigma, \quad (11)$$

where

$$K(e(\mathbf{q}), \alpha, k, T) = \frac{k}{1 + \exp(-\alpha(e(\mathbf{q}) - T))}, \quad (12)$$

where k determines the amplitude value of the *Sigmoid* function, and $e(\mathbf{q})$ is the local entropy centered at \mathbf{q} in an $m \times n$ neighborhood. α controls the width and monotonicity of the *Sigmoid* function. To be specific, if $\alpha < 0$, $K(e(\mathbf{q}), \alpha, k, T)$ is monotonically decreasing; if $\alpha = 0$, $K(e(\mathbf{q}), \alpha, k, T)$ is a constant; if $\alpha > 0$, $K(e(\mathbf{q}), \alpha, k, T)$



Fig. 5. The nine tested images *Lena*, *Barbara*, *Boat*, *Pepper*, *Cameraman*, *House*, *Hill*, *Man* and *Montage*.

α, k, T) is monotonically increasing. T is a threshold separating the heterogeneous areas and homogeneous areas.

4.3. The proposed EBF based denoising framework

After obtaining the new range kernel \hat{w}_{σ_r} in (10), then the proposed EBF can be written as

$$\hat{y}(\mathbf{q}) = \frac{\sum_{\mathbf{p} \in \mathcal{S}} w_{\sigma_s} \cdot \hat{w}_{\sigma_r} \cdot y(\mathbf{p})}{\sum_{\mathbf{p} \in \mathcal{S}} w_{\sigma_s} \cdot \hat{w}_{\sigma_r}}. \quad (13)$$

In order to apply the proposed EBF to image denoising, a two-stage EBF based denoising framework is presented in Fig. 4. It can be observed that the first stage consists of BF filtering and local entropy computing, and then outputs a denoised estimate, the corresponding method noise and local entropy map for the use of the proposed EBF in the second stage. Specifically, the denoised estimate and method noise are used to produce a new range distance to improve the robustness. At the same time, local entropy map is used to adaptively tune the range parameter. Then the proposed EBF denoises the noisy image and outputs the final denoised image.

For clarity, the denoising process is detailed in Algorithm 1.

Algorithm 1 The proposed EBF based denoising framework.

Input: Noisy image \mathbf{y} with noise variance σ^2

Output: Denoised image $\hat{\mathbf{y}}$

- 1: $\hat{\mathbf{x}} \leftarrow$ Apply BF to generate a denoised estimate via (1);
 - 2: $\hat{\mathbf{n}} \leftarrow$ Obtain method noise using (5);
 - 3: **for** each pixel \mathbf{q} in $\hat{\mathbf{y}}$ **do**
 - 4: $e(\mathbf{q}) \leftarrow$ Calculate local entropy of \mathbf{y} using (7);
 - 5: $\hat{\sigma}_r \leftarrow$ Compute the range parameter via (11);
 - 6: $\Delta x(\mathbf{q}) \leftarrow$ Extract the residual image from $\hat{\mathbf{x}}$ by Wiener filter;
 - 7: $|x(\mathbf{q}) - x(\mathbf{p})|^2 \leftarrow$ Estimate the new range distance between the pixel $x(\mathbf{q})$ and $x(\mathbf{p})$ via (9);
 - 8: $\hat{w}_{\sigma_r} \leftarrow$ Compute the new range kernel using (10);
 - 9: $\hat{y}(\mathbf{q}) \leftarrow$ Obtain the denoised result of $y(\mathbf{q})$ using (13).
 - 10: **end for**
 - 11: $\hat{\mathbf{y}} \leftarrow$ Return the denoised image.
-

5. Experimental results

5.1. Setup

As baselines, we use the standard BF [1], robust BF (RBF) [3], recently developed optimally weighted BF (WBF) [6] and multiresolution BF (MBF) [2]. All the experiments are tested on commonly used test images from the standard image dataset³, which presents a wide range of edges, textures and details and are shown in Fig. 5. Each image is contaminated with AWGN at $\sigma \in [10, 20, 30, 40, 50]$, and the intensity value for each pixel of the image ranges from 0 to 255. For the baseline algorithms, we set the following parameters: $\sigma_s = 1.8$, and the kernel radius $r = 5$. The critical range parameter is set to $\sigma_r = k\sigma$. In the case of BF, we set $\sigma_r = 1.95 \times \sigma$ recommended by Liu et al. [44]. For RBF and WBF, we tune the k to obtain the better results. Other parameters are set as the default parameter settings in the original literature [1–3,6].

For the proposed EBF, the window size are set to 11×11 , 3×3 for the local entropy computing and Wiener filter, respectively; for the range parameter $\hat{\sigma}_r = K(e(\mathbf{q}), \alpha, k, T) \cdot \sigma$, we set $\alpha = -1$ and $k = 2.5$ empirically. T is a threshold recommended by Yan et al. [45], i.e., $T = 0.7 \cdot e_{\max}$, where e_{\max} is the maximal local entropy of the entropy map. The influence of the parameters is discussed in the following parts. In the case of BF in our denoising framework, BF with $\sigma_r = 6 \times \sigma$ in the first stage turns out to be a better choice in terms of PSNR values.

5.2. Evaluation criteria

Two objective criteria, namely Peak Signal-to-Noise Ration (PSNR) and Feature similarity index (FSIM) [46], are used to evaluate the denoising results. Given two images \mathbf{x} and \mathbf{y} , PSNR can be computed as follows:

$$\text{PSNR}(\mathbf{x}, \mathbf{y}) = 10 \log_{10} \frac{S^2}{\text{MSE}}, \quad (14)$$

where $\text{MSE}(\mathbf{x}, \mathbf{y}) = 1/N \sum_{n=1}^N (x_n - y_n)^2$, where N is the number of pixels in a image; S is the dynamic range of allowable image pixel intensities. For an 8-bit gray-level image, $S = 255$.

As a complementary metric to PSNR, FSIM is a metric conceived to simulate the response of the human visual system (HVS), which can better reflect the structure similarity between the reference

³ http://www.cs.tut.fi/~foi/GCF-BM3D/index.html#ref_software

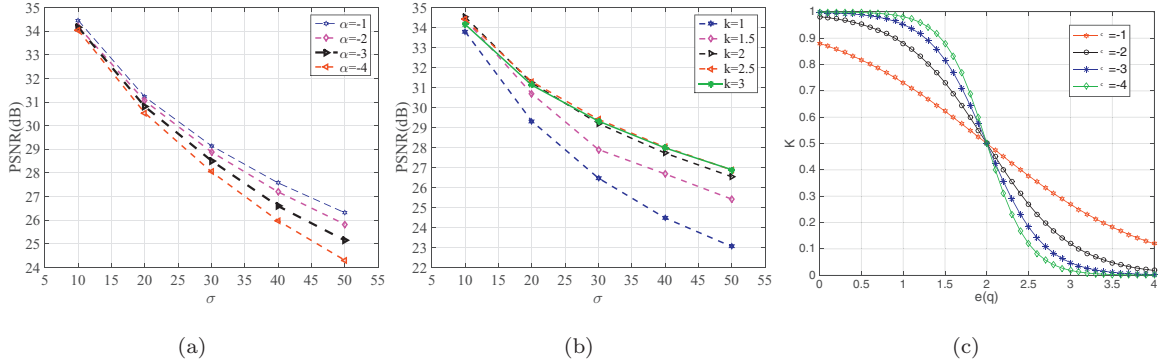


Fig. 6. Variations of the PSNR for different parameter values for the new range kernel with (a) different α ($k = 2$), and (b) different k ($\alpha = -1$). (c) An example of the curves for the function $K(e(q), \alpha, k, T)$ with various α ($e(q) \in [0, 4]$, $k = 2$, $T = 2$).

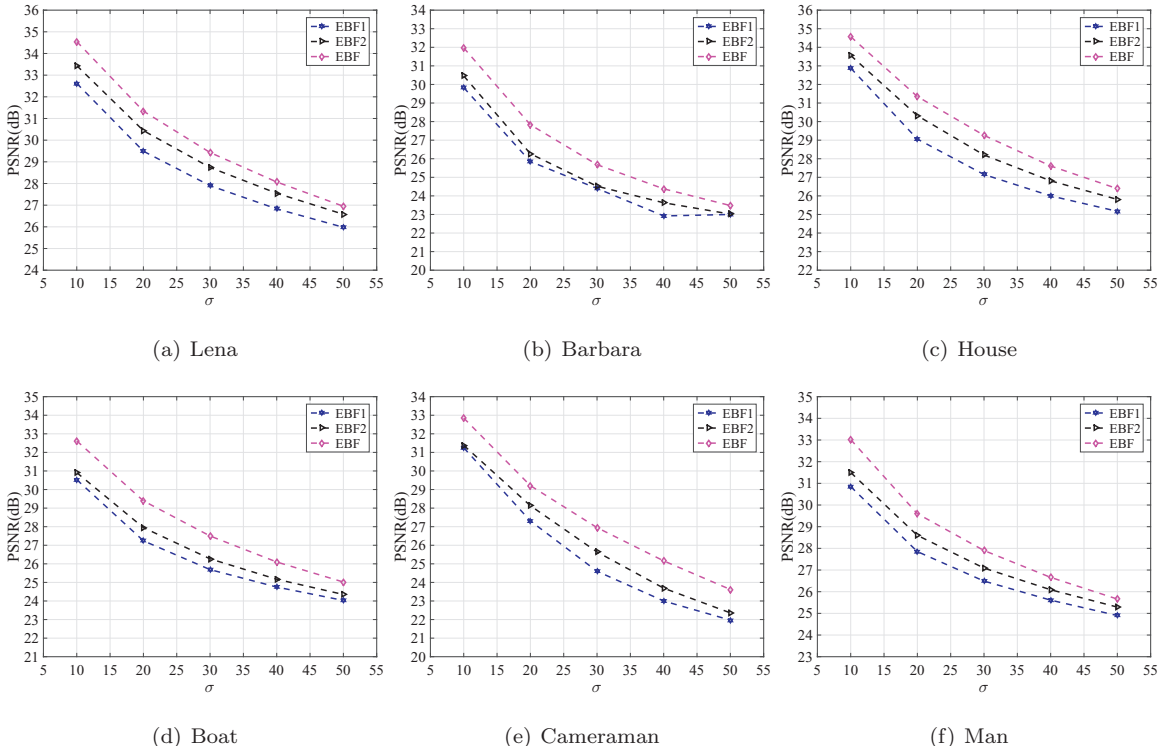


Fig. 7. PSNR values of the proposed method with the traditional range distance derived from the noisy image and fixed range parameter: $\hat{\sigma}_r = 2\sigma$ (EBF1), with the new range distance and fixed range parameter: $\hat{\sigma}_r = 2\sigma$ (EBF2), and with the new range distance and adaptive $\hat{\sigma}_r$ based on local entropy (EBF).

image and the target image. Given two images \mathbf{x} and \mathbf{y} , FSIM can be calculated as follows:

$$\text{FSIM}(\mathbf{x}, \mathbf{y}) = \frac{\sum_{i \in \Omega} S_L(i) \cdot PC_m(i)}{\sum_{i \in \Omega} PC_m(i)}, \quad (15)$$

where Ω means the whole image spatial domain, S_L measures the similarity of phase congruency (PC) and gradient magnitude (GM) features; PC_m is the maximal PC feature among all the PC features. For more details about FSIM refer to [46].

5.3. Effects of the new range kernel and parameter analysis

The function $K(e(q), \alpha, k, T)$ introduces three basic parameters: the scaling factor α , the amplitude value k and the position parameter T . Among them, we set $T = 0.7 \cdot e_{\max}$ which is recommended by Yan et al. [45]. The α determines the shrinkage direction and rate of the $K(e(q), \alpha, k, T)$. In order to remove the noise better, it is necessary to satisfy the condition that the larger the local entropy, the smaller the range parameter. That is, α should

be smaller than zero. Let us show intuitively the effect of α . An example of the curves for the $K(e(q), \alpha, k, T)$ with different α is shown in Fig. 6(c), where we can see that the larger α values, the flatter curves of the $K(e(q), \alpha, k, T)$. Moreover, from Fig. 6(a), we can see that our method is sensitive to the α selections at higher noise levels. This is because the discrimination of different areas on entropy tends to become weak (see Table 1), which then results in unreliable estimation of the range parameter. In this case, it is more reasonable to use the flatter curve of the $K(e(q), \alpha, k, T)$, which corresponds to small variations of the range parameter. Empirically, $\alpha = -1$ achieves the best results. Similarly, we show the PSNR curves for varying k and fixed $\alpha = -1$ in Fig. 6(b). It can be seen that the best result is obtained with $k = 2.5$.

In order to better illustrate the effects of the new range kernel \hat{w}_{σ_r} in various noise levels for different images, we categorize \hat{w}_{σ_r} into three cases: the traditional range distance $|y(\mathbf{p}) - y(\mathbf{q})|^2$ with fixed $\hat{\sigma}_r$ (EBF1), the new range distance $|x(\mathbf{p}) - x(\mathbf{q})|^2$ with fixed $\hat{\sigma}_r$ (EBF2), and the new range distance $|x(\mathbf{p}) - x(\mathbf{q})|^2$ with adap-

Table 2

PSNR values of BF [1], RBF [3], WBF [6], MBF [2] and the proposed EBF with various tested images for various values of σ . The top PSNR results for each image and on each noise level are highlighted in bold.

	σ	10	20	30	40	50	Average
Lena (512 × 512)	BF	33.61/0.9777	29.80/0.9448	27.25/0.9037	25.36/0.8623	23.88/0.8252	27.98/0.9027
	RBF	34.10/0.9785	31.43/0.9508	29.56/0.9222	28.08/0.8876	26.93/0.8580	30.02/0.9194
	WBF	34.61 /0.9789	31.51 /0.9500	29.58 /0.9213	28.09 /0.8871	26.19/0.8579	29.99/0.9190
	MBF	34.06/0.9714	30.98/0.9494	29.26/0.9313	28.02/ 0.9159	27.16 / 0.9034	29.89/0.9342
Barbara (512 × 512)	EBF	34.55 / 0.9790	31.33 / 0.9572	29.45 / 0.9357	28.06/0.9141	26.92/0.8937	30.06 / 0.9359
	BF	31.39/0.9765	27.11/0.9412	24.90/0.9039	23.40/0.8679	22.27/0.832	25.81/0.9043
	RBF	28.47/0.9604	25.57/0.9223	24.27/0.8970	23.54/0.8761	23.00/0.8573	24.97/0.9026
	WBF	31.42/0.9766	27.24/0.9418	25.12/0.9045	24.00/0.8745	23.23/0.8512	26.20/0.9097
Boat (512 × 512)	MBF	31.39/0.9734	27.25/0.9447	25.24/0.9216	24.11/0.9014	23.45/0.8868	26.28/0.9255
	EBF	31.60 / 0.9770	27.68 / 0.9519	25.58 / 0.9303	24.32 / 0.9086	23.46 / 0.8893	26.53 / 0.9314
	BF	32.15/0.9741	28.45/0.9417	26.20/0.9082	24.50/0.8742	23.09/0.8419	26.87/0.9080
	RBF	31.52/0.9758	29.02/0.9465	27.44/0.9151	26.22/0.8871	25.23/0.8617	27.88/0.9172
Pepper (256 × 256)	WBF	32.63/0.9776	29.42/0.9457	27.58 /0.9143	26.26 /0.8858	25.25 /0.8606	28.22 /0.9168
	MBF	31.91/0.9664	28.64/0.9247	26.91/0.8933	25.74/0.8686	24.88/0.8488	27.61/0.9003
	EBF	32.65 / 0.9790	29.44 / 0.9498	27.47/ 0.9224	26.09/ 0.8962	25.00/ 0.8737	28.11/ 0.9242
	BF	33.09/0.9529	28.87/0.9082	26.25/0.8592	24.29/0.8118	22.78/0.7698	27.05/0.8603
Cameraman (256 × 256)	RBF	32.57/0.9453	29.86/0.9218	27.83/0.8932	26.25/0.8635	24.93/0.8406	28.28/0.8928
	WBF	33.59/ 0.9544	30.25 /0.9232	27.95 /0.8910	26.31 /0.8609	24.97 /0.8369	28.61 /0.8932
	MBF	32.98/0.9431	29.42/0.9069	27.29/0.8834	25.83/0.8658	24.59/0.8488	28.02/0.8896
	EBF	33.83 /0.9530	30.25 / 0.9249	27.86/ 0.9011	25.98/ 0.8767	24.47/ 0.8532	28.48/ 0.9018
House (256 × 256)	BF	32.72/0.9426	28.46/0.8836	25.86/0.8278	23.87/0.7745	22.43/0.7338	26.66/0.8324
	RBF	30.39/0.9201	27.22/0.8712	25.87/0.8386	24.80/0.8166	23.77/0.7860	26.41/0.8465
	WBF	32.76 /0.9430	28.81/0.8893	26.61/0.8423	25.10/0.8105	23.91/0.7791	27.43/0.8528
	MBF	32.09/0.9267	28.51/0.8664	26.55/0.8357	25.10/0.8121	24.03 /0.7919	27.25/0.8465
Hill (512 × 512)	EBF	32.74/ 0.9451	29.20 / 0.8990	26.99 / 0.8692	25.20 / 0.8427	23.71/ 0.8158	27.57 / 0.8743
	BF	33.79/0.9435	29.61/0.8955	26.97/0.8369	25.19/0.7874	23.58/0.7428	27.82/0.8412
	RBF	33.93/0.9342	31.28/0.9068	29.40/0.8818	27.78 /0.8527	26.55/0.8273	29.78/0.8805
	WBF	34.59 / 0.9436	31.39 / 0.9088	29.41 /0.8814	27.78 /0.8520	26.55/0.8271	29.94 /0.8825
Man (512 × 512)	MBF	34.18/0.9206	31.21/0.8908	29.23/0.8663	27.73/0.8447	26.74 /0.8291	29.81/0.8703
	EBF	34.48/0.9399	31.27/0.9064	29.22/ 0.8835	27.65/ 0.8600	26.40/ 0.8373	29.81/ 0.8854
	BF	32.24/0.9711	28.77/0.9375	26.64/0.9036	24.96/0.8699	23.49/0.8326	27.22/0.9029
	RBF	31.74/0.9714	29.39/0.9424	27.99/0.9115	26.92/0.8826	26.07/0.8596	28.42/0.9135
Montage (256 × 256)	WBF	32.66 /0.9737	29.68 /0.9419	28.08 /0.9104	26.95 /0.8816	26.08 /0.8591	28.69 /0.9133
	MBF	31.78/0.9600	28.83/0.9180	27.42/0.8876	26.52/0.8675	25.82/0.8478	28.07/0.8961
	EBF	32.42/ 0.9758	29.48/ 0.9443	27.87/ 0.9198	26.77/ 0.8968	25.91/ 0.8795	28.49/ 0.9232
	BF	32.45/0.9728	28.78/0.9393	26.52/0.9054	24.81/0.8711	23.33/0.8395	27.17/0.9056
	RBF	32.01/0.9741	29.53/0.9452	27.96/0.9159	26.75/0.8842	25.83/0.8617	28.41/0.9162
	WBF	32.98/0.9763	29.81 /0.9443	28.05 /0.9147	26.77 /0.8830	25.84 /0.8610	28.69 /0.9158
	MBF	32.10/0.9631	28.92/0.9222	27.30/0.8920	26.26/0.8703	25.52/0.8536	28.02/0.9002
	EBF	33.05 / 0.9777	29.70/ 0.9458	27.92/ 0.9205	26.68/ 0.8978	25.68/ 0.8792	28.61/0.9242
	BF	34.62/0.9514	30.04/0.8881	27.20/0.8240	24.84/0.7582	23.15/0.7063	27.97/0.8256
	RBF	32.49/0.9359	29.76/0.8968	27.63/0.8493	26.02/0.8283	24.77/0.7918	28.13/0.8604
	WBF	34.86/0.9508	30.88/0.8984	28.32/0.8452	26.43/0.8130	24.93/0.7786	29.08/0.8572
	MBF	34.61/0.9484	30.90/0.9168	28.67/0.8930	26.83/0.8732	25.52/0.8557	29.30/0.8974
	EBF	35.83 / 0.9596	31.95 / 0.9328	29.30 / 0.9049	26.99 / 0.8739	25.01 / 0.8434	29.80 / 0.9029

tive $\hat{\sigma}_r$ (EBF). From Fig. 7, we can see that EBF2 obtains higher PSNR values than EBF1 in most cases, which demonstrates the effectiveness of the new range distance $|x(\mathbf{p}) - x(\mathbf{q})|^2$. It is worth mentioning that for image *Barbara* shown in Fig. 7(b), EBF2 obtains a small amount of improvement compared with EBF1. This is because rich textures are distributed in the image *Barbara* and can be easily smoothed by BF in the first stage. Moreover, EBF further improves the PSNR values over EBF2. This is because our adaptive $\hat{\sigma}_r$ captures the varying local geometry, thus leading to better performance.

5.4. Comparison with other denoising methods

5.4.1. Quantitative metrics

In Table 2, we quantify the performance of various denoising methods for the test images at various noise levels in terms of PSNR and FSIM. The best results are set in bold. For FSIM, it can be observed that the proposed EBF obtains the best results in most cases, which implies the advantage of EBF in preserving the image structures. For PSNR, we can see that EBF achieves the best results for some images, such as the images *Barbara*, *Cameraman*, and *Montage*. The proposed EBF and WBF obtain comparable performance in terms of PSNR, and outperform other denoising methods

in most cases. Besides, BF works well at low noise levels, while RBF and MBF perform well at high noise levels. This is the reason why WBF can remove the noise effectively at various noise levels, since WBF can take advantage of BF and RBF in an optimally weighted fashion. In addition, it should be noted that our method performs better on images with rich repeated patterns and textured regions such as *Barbara*, *Boat* and *Montage*.

5.4.2. Visual quality

To evaluate the visual quality of various methods, we show the denoised and zoom-in results of the four images (at $\sigma = 30$) in Figs. 8 and 9. It can be seen that EBF and MBF have better visual effects than other denoising methods. Specifically, MBF produces smoother images. This is explained that MBF combines BF and wavelet thresholding, where BF is applied to the approximation subbands to eliminate low-frequency noise components. Instead, the proposed EBF has more artifacts, but it performs better at the local structures (e.g. the masts of the image *Boat* and the scarf of the image *Barbara*). This is explained that EBF adopts a new range distance to embed the information from the residual image and the denoised estimate, and uses adaptive range parameter to better keep the image local structures. Among all the testing methods, BF with the fixed range parameter has the worst visual



Fig. 8. Denoised and zoom-in results with different algorithms for *Lena* and *Barbara* at $\sigma = 30$.

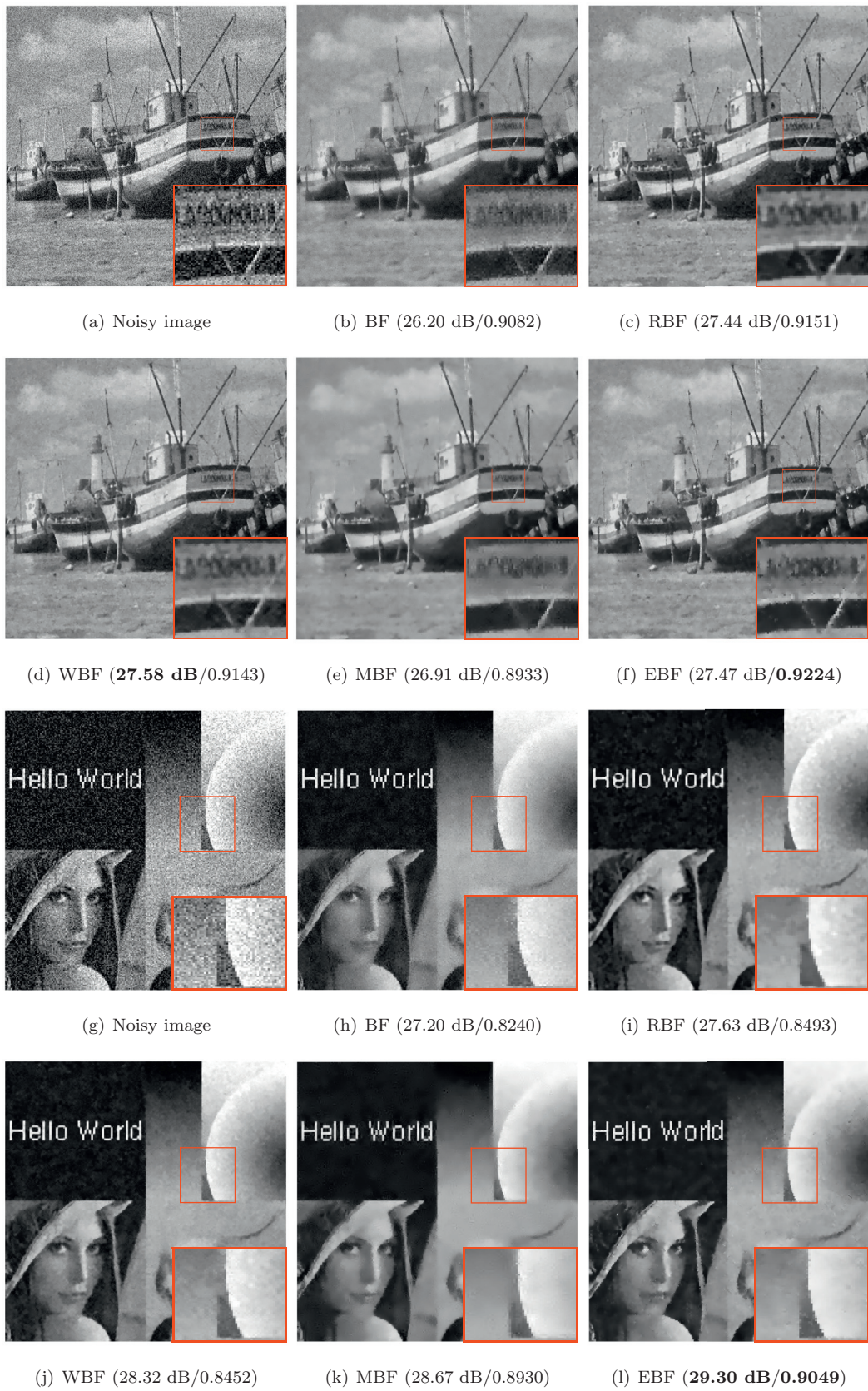


Fig. 9. Denoised and zoom-in results with different algorithms for *Boat* and *Montage* at $\sigma = 30$.

Table 3

Time complexity of various algorithms. $N = \#$ pixel number of an image, $r = \#$ the kernel radius, $L_e = \#$ window size of entropy computation, $L_w = \#$ window size of Wiener filter, and $M = \#$ wavelet filter length.

Time complexity	
BF	$O(N \cdot r^2)$
RBF	$O(N \cdot r^2)$
WBF	$O(N^2)$
MBF	$O(N^2(M \cdot \log_2 N + 1 + r^2))$
Ours	$O(N(r^2 + L_e^2 + L_w^2))$

quality, while EBF with adaptive range parameter excels in preserving fine structures of images.

5.5. Computational complexity

Our EBF based denoising framework can be divided into two stages. Most of the computational cost spends on local entropy computation, Wiener filter and the double application of BF, and thus the complexity mainly depends on: the window size L_e , L_w and the kernel radius r of entropy computation, Wiener filter and BF, respectively. For each pixel, it requires $O(L_e^2)$, $O(L_w^2)$ and $O(r^2)$ time implementations for entropy computation, Wiener filter and BF, respectively. Therefore, for an image with N pixels, the time complexity of the proposed method is $O(N(L_e^2 + L_w^2 + r^2))$.

To give a more intuitive comparison, the time complexity of different denoising algorithms is summarized in Table 3. Among these algorithms, MBF has the highest time complexity due to the fact that it integrates wavelet thresholding and BF into a denoising framework. Our method has only a little higher time complexity than RBF and BF. In practice, L_w and L_e are close to r , therefore, we can get better quality denoising images with little loss of computation time.

6. Conclusions

In this paper, an adaptive entropy-based BF (EBF) with a new range kernel is proposed, which consists of a new range distance and adaptive range parameter selections. Specifically, the new range distance is derived from the approximately clean pixels, which exploits pixel similarities between the denoised image and its residual image. With the new range distance, EBF can handle various noise levels. In order to consider the local structures of images, local entropy serves as a guide to tune the range parameter, which makes our method adapt to the images with different characteristics. Due to the new range kernel, the proposed EBF keeps the local structures of images effectively. Experimental results demonstrate that the proposed EBF significantly outperforms the standard BF with little loss of computation time.

Acknowledgements

This work is supported by the National Natural Science Foundation of China under grant No. 61371078, and the R&D Program of Shenzhen under grant Nos. JCYJ20140509172959977, JS20150512162853495, ZDSYS20140509172959989, JCYJ20160331184440545.

References

- [1] C. Tomasi, R. Manduchi, Bilateral filtering for gray and color images, in: 1998 IEEE International Conference on Computer Vision, IEEE, 1998, pp. 839–846.
- [2] M. Zhang, B.K. Gunturk, Multiresolution bilateral filtering for image denoising, IEEE Trans. Image Process. 17 (12) (2008) 2324–2333.
- [3] G. Petschnigg, R. Szeliski, M. Agrawala, M. Cohen, H. Hoppe, K. Toyama, Digital photography with flash and no-flash image pairs, ACM Trans. Graph. 23 (3) (2004) 664–672.
- [4] H. Yu, L. Zhao, H. Wang, Image denoising using trivariate shrinkage filter in the wavelet domain and joint bilateral filter in the spatial domain, IEEE Trans. Image Process. 18 (10) (2009) 2364–2369.
- [5] K. He, J. Sun, X. Tang, Guided image filtering, IEEE Trans. Pattern Anal. Mach. Intell. 35 (6) (2013) 1397–1409.
- [6] K.N. Chaudhury, K. Rithwik, Image denoising using optimally weighted bilateral filters: a sure and fast approach, in: 2015 IEEE International Conference on Image Processing, IEEE, 2015, pp. 108–112.
- [7] A. Buades, B. Coll, J.-M. Morel, A non-local algorithm for image denoising, in: 2005 IEEE Computer Society Conference on Computer Vision and Pattern Recognition, IEEE, 2005, pp. 60–65.
- [8] B. Zhang, J.P. Allebach, Adaptive bilateral filter for sharpness enhancement and noise removal, IEEE Trans. Image Process. 17 (5) (2008) 664–678.
- [9] I. Frolio, K. Egiazarian, K. Pulli, Machine learning for adaptive bilateral filtering, IS&T/SPIE Electronic Imaging, International Society for Optics and Photonics, 2015. 939908–939908.
- [10] S. Ling, Y. Ruomei, L. Xuelong, L. Yan, From heuristic optimization to dictionary learning: a review and comprehensive comparison of image denoising algorithms, IEEE Trans. Cybern. 44 (7) (2014) 1001–1013.
- [11] X. Li, Y. Hu, X. Gao, D. Tao, B. Ning, A multi-frame image super-resolution method, Signal Process. 90 (2) (2010) 405–414.
- [12] P. Perona, J. Malik, Scale-space and edge detection using anisotropic diffusion, IEEE Trans. Pattern Anal. Mach. Intell. 12 (7) (1990) 629–639.
- [13] L.I. Rudin, S. Osher, E. Fatemi, Nonlinear total variation based noise removal algorithms, Physica D 60 (1) (1992) 259–268.
- [14] Y. Hao, J. Xu, J. Bai, Y. Han, Image decomposition combining a total variational filter and a tikhonov quadratic filter, Multidimens. Syst. Signal Process. 26 (3) (2015) 739–751.
- [15] Z. Su, X. Luo, Z. Deng, Y. Liang, Z. Ji, Edge-preserving texture suppression filter based on joint filtering schemes, IEEE Trans Multimedia 15 (3) (2013) 535–548.
- [16] K. Dabov, A. Foi, V. Katkovnik, K. Egiazarian, Image denoising by sparse 3-d transform-domain collaborative filtering, IEEE Trans. Image Process. 16 (8) (2007) 2080–2095.
- [17] L. Zhang, W. Dong, D. Zhang, G. Shi, Two-stage image denoising by principal component analysis with local pixel grouping, Pattern Recognit. 43 (4) (2010) 1531–1549.
- [18] T. Dai, C.-B. Song, J.-P. Zhang, S.-T. Xia, PMPA: a patch-based multiscale products algorithm for image denoising, in: 2015 IEEE International Conference on Image Processing, IEEE, 2015, pp. 4406–4410.
- [19] M. Elad, M. Aharon, Image denoising via sparse and redundant representations over learned dictionaries, IEEE Trans. Image Process. 15 (12) (2006) 3736–3745.
- [20] J. Mairal, F. Bach, J. Ponce, G. Sapiro, A. Zisserman, Non-local sparse models for image restoration, in: 2009 IEEE International Conference on Computer Vision, 2009, pp. 2272–2279.
- [21] D. Zoran, Y. Weiss, From learning models of natural image patches to whole image restoration, in: 2011 IEEE International Conference on Computer Vision, IEEE, 2011, pp. 479–486.
- [22] S. Gu, L. Zhang, W. Zuo, X. Feng, Weighted nuclear norm minimization with application to image denoising, in: 2014 IEEE Computer Society Conference on Computer Vision and Pattern Recognition, IEEE, 2014, pp. 2862–2869.
- [23] H.C. Burger, C.J. Schuler, S. Harmeling, Image denoising: can plain neural networks compete with bm3d? in: 2012 IEEE Conference on Computer Vision and Pattern Recognition, 2012, pp. 2392–2399.
- [24] R. Wang, D. Tao, Non-local auto-encoder with collaborative stabilization for image restoration, IEEE Trans. Image Process. 25 (5) (2016) 2117–2129.
- [25] M. Elad, On the origin of the bilateral filter and ways to improve it, IEEE Trans. Image Process. 11 (10) (2002) 1141–1151.
- [26] D. Barash, Fundamental relationship between bilateral filtering, adaptive smoothing, and the nonlinear diffusion equation, IEEE Trans Pattern Anal Mach Intell 24 (6) (2002) 844–847.
- [27] S. Farsiu, M.D. Robinson, M. Elad, P. Milanfar, Fast and robust multiframe super resolution, IEEE Trans. Image Process. 13 (10) (2004) 1327–1344.
- [28] P. Mrázek, J. Weickert, A. Bruhn, On Robust Estimation and Smoothing with Spatial and Tonal Kernels, Springer, 2006.
- [29] H. Takeda, S. Farsiu, P. Milanfar, Kernel regression for image processing and reconstruction, IEEE Trans. Image Process. 16 (2) (2007) 349–366.
- [30] L. Caraffa, J.-P. Tarel, P. Charbonnier, The guided bilateral filter: when the joint/cross bilateral filter becomes robust, IEEE Trans. Image Process. 24 (4) (2015) 1199–1208.
- [31] F. Durand, J. Dorsey, Fast bilateral filtering for the display of high-dynamic-range images, ACM Trans. Graph. 21 (3) (2002) 257–266.
- [32] S. Paris, F. Durand, A fast approximation of the bilateral filter using a signal processing approach, in: Computer Vision 2006, Springer, 2006, pp. 568–580.
- [33] F. Porikli, Constant time o(1) bilateral filtering, in: 2008 IEEE Conference on Computer Vision and Pattern Recognition, IEEE, 2008, pp. 1–8.
- [34] K.N. Chaudhury, D. Sage, M. Unser, Fast bilateral filtering using trigonometric range kernels, IEEE Trans. Image Process. 20 (12) (2011) 3376–3382.
- [35] K.N. Chaudhury, Acceleration of the shiftable algorithm for bilateral filtering and nonlocal means, IEEE Trans. Image Process. 22 (4) (2013) 1291–1300.
- [36] S. Ghosh, K.N. Chaudhury, On fast bilateral filtering using fourier kernels, IEEE Signal Process. Lett 23 (5) (2016) 570–573.
- [37] K.N. Chaudhury, S.D. Dabhade, Fast and provably accurate bilateral filtering, IEEE Trans. Image Process. 25 (6) (2016) 2519–2528.

- [38] C.E. Shannon, A mathematical theory of communication, *ACM SIGMOBILE Mobile Comput. Commun. Rev.* 5 (1) (2001) 3–55.
- [39] J.N. Kapur, P.K. Sahoo, A.K. Wong, A new method for gray-level picture thresholding using the entropy of the histogram, *Comput. Vis. Graph. Image Process.* 29 (3) (1985) 273–285.
- [40] D. Brunet, E.R. Vrcay, Z. Wang, The use of residuals in image denoising, in: *Image Analysis and Recognition*, Springer, 2009, pp. 1–12.
- [41] S. Paris, P. Kornprobst, J. Tumblin, F. Durand, *Bilateral Filtering: Theory and Applications*, Now Publishers Inc, 2009.
- [42] M.A. El-Sayed, Edges detection based on renyi entropy with split/merge, *Comput. Eng. Intell. Syst.* 3 (9) (2012) 32–41.
- [43] A. Fathi, A.R. Naghsh-Nilchi, Efficient image denoising method based on a new adaptive wavelet packet thresholding function, *IEEE Trans. Image Process.* 21 (9) (2012) 3981–3990.
- [44] C. Liu, W.T. Freeman, R. Szeliski, S.B. Kang, Noise estimation from a single image, in: *2006 IEEE Computer Society Conference on Computer Vision and Pattern Recognition*, IEEE, 2006, pp. 901–908.
- [45] C. Yan, N. Sang, T. Zhang, Local entropy-based transition region extraction and thresholding, *Pattern Recognit. Lett.* 24 (16) (2003) 2935–2941.
- [46] L. Zhang, L. Zhang, X. Mou, D. Zhang, Fsim: a feature similarity index for image quality assessment, *IEEE Trans. Image Process.* 20 (8) (2011) 2378–2386.